Observing Topological Invariants Using Quantum Walks in Superconducting Circuits

E. Flurin,[1,2,*] V. V. Ramasesh,[1,2] S. Hacohen-Gourgy,[1,2] L. S. Martin,[1,2] N. Y. Yao,[1] and I. Siddiqi[1,2]

[1]*Department of Physics, University of California, Berkeley, California 94720, USA*

[2]*Center for Quantum Coherent Science, University of California, Berkeley, California 94720, USA*

(Received 6 December 2016; revised manuscript received 12 May 2017; published 3 August 2017)

The direct measurement of topological invariants in both engineered and naturally occurring quantum materials is a key step in classifying quantum phases of matter. Here, we motivate a toolbox based on time-dependent quantum walks as a method to digitally simulate single-particle topological band structures. Using a superconducting qubit dispersively coupled to a microwave cavity, we implement two classes of split-step quantum walks and directly measure the topological invariant (winding number) associated with each. The measurement relies upon interference between two components of a cavity Schrödinger cat state and highlights a novel refocusing technique, which allows for the direct implementation of a digital version of Bloch oscillations. As the walk is performed in phase space, our scheme can be extended to higher synthetic dimensions by adding additional microwave cavities, whereby superconducting circuit-based simulations can probe topological phases ranging from the quantum-spin Hall effect to the Hopf insulator.

DOI: 10.1103/PhysRevX.7.031023

Subject Areas: Quantum Physics, Quantum Information, Topological Insulators

Topological phases elude the Landau-Ginzburg paradigm of symmetry breaking [1]. Unlike conventional phases, they do not exhibit order parameters that can be locally measured. Rather, their distinguishing features are hidden in quantized, nonlocal topological invariants, which are robust to all local perturbations [2,3]. While tremendous theoretical progress has been made toward the full classification of topological phases of matter [4,5], a general experimental platform for the direct measurement of topological invariants is lacking. Here, we demonstrate that time-dependent quantum walks comprise a powerful class of unitary protocols capable of digitally simulating single-particle topological band structures and directly observing the associated nonlocal invariants.

A quantum walk [6–11] describes the motion of a particle with internal (spin) degrees of freedom moving on a discrete lattice. Formally, the quantum walk is comprised of two unitary operations [see Fig. 1(a)]: a coin toss, denoted $\hat{R}(\theta)$, which rotates the spin state, and a spin-dependent translation, denoted $\hat{T}_{\uparrow\downarrow}$, which translates the particle's position by a single lattice site in a direction determined by the internal spin state. In our cavity quantum electrodynamics implementation of the quantum walk, the particle is encoded as a coherent state of an electromagnetic cavity mode [12,13], where its position is defined in the cavity's phase space, as shown in Fig. 1(b). Its spin degrees of freedom are formed by a superconducting transmon qubit [14] with basis states $\{|\uparrow\rangle, |\downarrow\rangle\}$. To enable the qubit state to control the direction of motion of the coherent state, we realize a strong dispersive coupling between the cavity and qubit,

$$\hat{H}/\hbar = \omega_q \hat{\sigma}_z/2 + \omega_c \hat{a}^\dagger \hat{a} - \chi_{qc} \hat{a}^\dagger \hat{a} \hat{\sigma}_z/2, \qquad (1)$$

where $\omega_{q,c}$ are the qubit and cavity transition frequencies, respectively, $\hat{a}$ ($\hat{a}^\dagger$) is the lowering (raising) operator for the cavity mode, σ_z is the Pauli z matrix for the qubit levels, and χ_{qc} is the dispersive interaction strength [see Fig. 1(c)]. Dispersive coupling produces a qubit-dependent shift in the cavity oscillation frequency. Viewed in the rotating frame of the cavity at ω_c, the dispersive interaction causes the coherent state to move clockwise (counterclockwise) at a rate $\chi_{qc}/2$ through phase space when the qubit is in the $|\uparrow\rangle$ ($|\downarrow\rangle$) state. Thus, free evolution under the dispersive interaction precisely enables the spin-dependent translation needed for the quantum walk [15,16].

We realize a particular class of quantum algorithm known as the split-step quantum walk [17,18], which alternates two coin tosses (with rotation angles θ_1 and θ_2) between two spin-dependent translations so that each step of the walk consists of the unitary operation $\hat{U}_W(\theta_1, \theta_2) = \hat{T}_{\uparrow\downarrow}\hat{R}(\theta_2)\hat{T}_{\uparrow\downarrow}\hat{R}(\theta_1)$ [see Fig. 1(a)]. The coin-toss operations $\hat{R}_x(\theta) = e^{i\theta\hat{\sigma}_x/2}$ are applied via short (7.5-ns) coherent microwave pulses resonant with the qubit transition. By waiting for a time interval $t = 2\pi(10\chi_{qc})^{-1} = 124$ ns between successive coin tosses, we allow the dispersive

*emmanuel.flurin@berkeley.edu

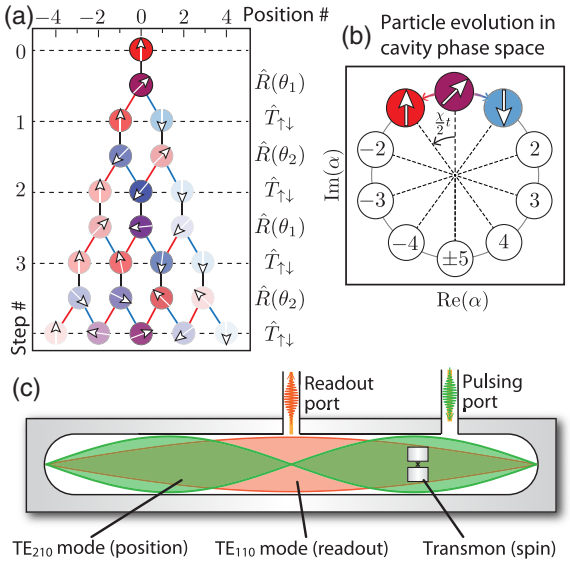

FIG. 1. Quantum-walk implementation in cavity phase space. (a) Schematic representation of a split-step quantum walk on a line, with rotations $\hat{R}(\theta_1)$ and $\hat{R}(\theta_2)$ and spin-dependent translation $T_{\uparrow\downarrow}$. Red (blue) lines show spin-up (-down) components moving left (right). The opacity of each circle indicates the population on the corresponding lattice site. (b) Set of ten cavity coherent states on which the walk takes place, in the phase space of the TE_{210} cavity mode. (c) Cavity resonator and qubit. The fundamental (TE_{110}, orange) mode at $\omega_R = 2\pi \times 6.77$ GHz is used to measure the qubit state. This mode couples strongly [$\kappa = 2\pi \times 600$ kHz $= 1/(260$ ns)] to a 50-ohm transmission line via the readout port at the center of the cavity. The TE_{210} cavity mode (green) at $\omega_c = 2\pi \times 7.41$ GHz is long lived with an inverse lifetime, $\kappa = 2\pi \times 4$ kHz $= 1/(40\ \mu$s). The transmon qubit (coin) has transition frequency $\omega_q = 2\pi \times 5.2$ GHz, relaxation times $T_1 = 40\ \mu$s and $T_2^* = 5.19\ \mu$s, and is dispersively coupled to both cavity modes, with the dispersive shift of the walker mode, $\chi_{qc} = 2\pi \times 1.61$ MHz.

coupling to naturally implement the spin-dependent translation. This time interval determines the lattice on which the walk takes place; here, it is a circular lattice of ten sites in cavity phase space [Fig. 1(b)].

We begin by performing a pair of topologically distinct split-step quantum walks, the first (topologically trivial) with unitary $\hat{U}_0 = \hat{U}_W(3\pi/4, \pi/4)$, and the second (topologically nontrivial) with $\hat{U}_1 = \hat{U}_W(\pi/4, 3\pi/4)$. To demonstrate the robustness of the winding number, we also implement an additional pair of walks which are continuously connected to $\hat{U}_0$ and $\hat{U}_1$ (e.g., without closing the gap). The experimental sequence is shown in Fig. 2(a). The cavity mode is initialized ($\mathcal{D}_\beta$) in a coherent state $|\beta\rangle$ with $|\beta|^2 = 8$ photons, after which the walk unitary is repeatedly applied. To directly reconstruct the walker's quantum state on the phase-space lattice, we first projectively measure the qubit state and subsequently measure the Q function of the cavity mode [19]. Figure 2(b) depicts the measured lattice site populations after each step of the walk. We observe the expected ballistic expansion of the coherent state in cavity phase space, consistent with theoretical predictions (population fidelities greater than 90%).

As the walk unitary $\hat{U}_W$ directly couples the particle's spin and position degrees of freedom, the resulting dynamics mimic those of spin-orbit interacting materials. More precisely, the unitary quantum-walk protocol simulates continuous evolution under an effective spin-orbit Hamiltonian $\hat{H}_W$, which generates the same transformation as a single step of the walk when $\hat{U}_W = e^{-i\hat{H}_W}$. Since the unitary is translation invariant, the effective Hamiltonian exhibits Bloch bands of quasienergy $\pm\epsilon(k)$, where the quasimomentum k lies in the Brillouin zone; Figs. 3(a) and 3(b) show, respectively, the band structures underlying the walks $\hat{U}_0$ and $\hat{U}_1$. The corresponding eigenstates consist of extended Bloch waves with spin polarization $\pm\vec{n}(k)$ [17]. Depending on symmetry, the band structure of such spin-orbit-coupled Hamiltonians can feature quantized topological invariants. In the case of the split-step quantum walk, $\Gamma = e^{-i\pi\vec{A}\cdot\vec{\sigma}/2}$ plays the role of a so-called chiral symmetry [17,20], with $\Gamma^\dagger \hat{U}_W \Gamma = -\hat{U}_W$. This symmetry constrains the spin polarization vector $\vec{n}(k)$ to lie on a great circle of the Bloch sphere, perpendicular to $\vec{A} = (\cos(\theta_1/2), 0, \sin(\theta_1/2))$ [Figs. 3(c) and 3(d)]. Thus, the number of times $\vec{n}(k)$ wraps around the origin as k varies through the Brillouin zone—known as the winding or Chern number $\mathcal{W}$—naturally defines the topological invariant [17] of the walk. While the energy spectra of $\hat{U}_0$ and $\hat{U}_1$ are identical, they lie in topologically distinct phases, with $\hat{U}_0$ having zero winding number and $\hat{U}_1$ a winding number of unity. Analogous to the number of twists in a closed ribbon, winding numbers are quantized and robust to local perturbations [2].

The direct measurement of topological invariants in solid-state materials is an outstanding challenge [21–23], owing to the nonlocal nature of the order parameter. Our method makes use of a time-dependent modification of the quantum walk, which, in the Hamiltonian picture, mimics an adiabatic translation of the underlying band structure across the Brillouin zone [24–28]. The resulting dynamics effectively constitute digital Bloch oscillations, a phenomenon whereby a particle on a lattice subjected to a constant force undergoes oscillations [29] due to the periodicity of the Brillouin zone. In our system, these oscillations manifest as a refocusing of the quantum walker to its initial position, with a Berry phase—a signature of the band-structure topology (see Fig. 3)—imprinted during the evolution. In practice, this refocusing depends on choosing the number of steps in the walk such that the accrued dynamical phase—which has opposite signs in either band and thus impedes refocusing—effectively vanishes [19,24]. In the general setting, one can experimentally determine the condition for dynamical phase refocusing by performing spectroscopy while varying the number of steps.

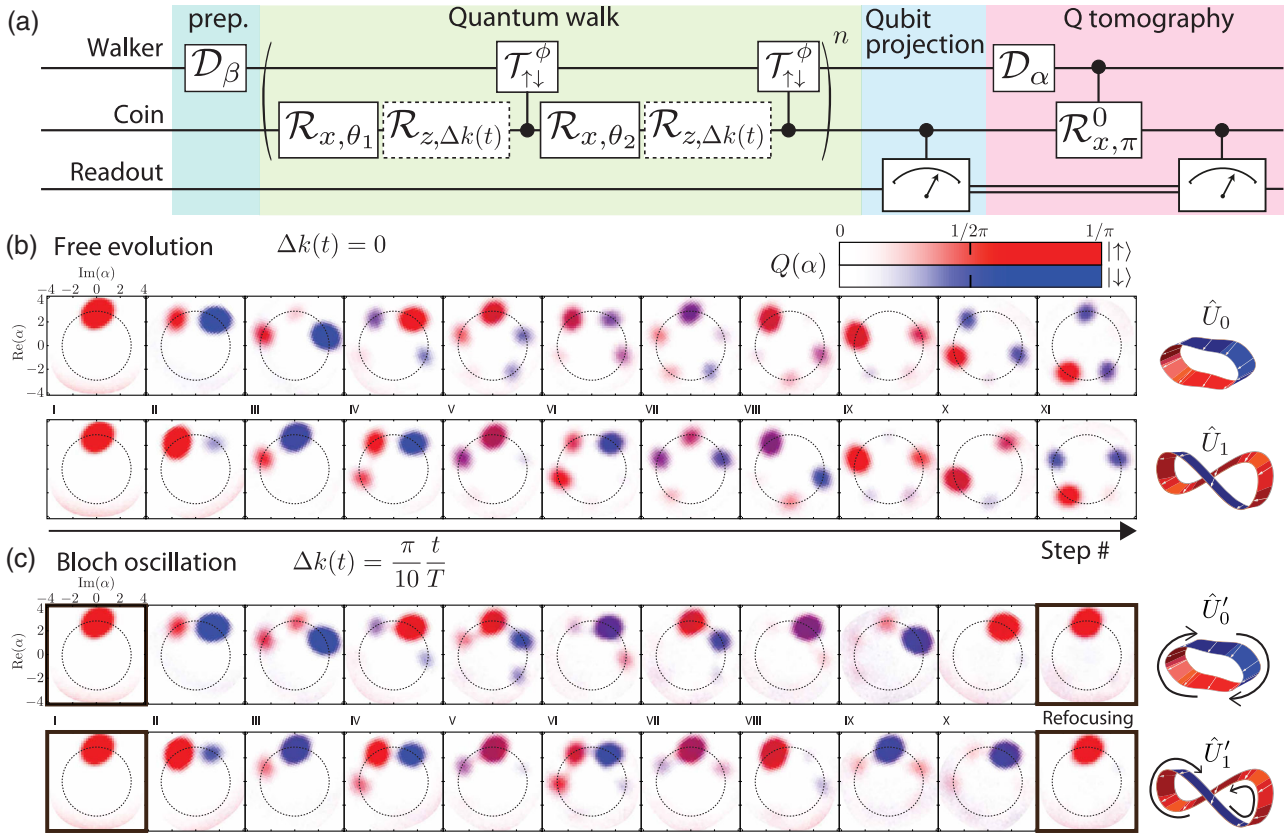

FIG. 2. Quantum-walk protocol and resulting populations. (a) Protocol used to perform the quantum walk, showing cavity state preparation (blue), quantum walk (green), qubit state measurement (blue), and Q function measurement (pink). The dashed boxes with σ_z gates are performed to implement the Bloch oscillation. (b) Cavity Q functions after each step of the quantum walk without Bloch oscillations, $\hat{U}_0$ (top strip) and $\hat{U}_1$ (bottom strip). Spin-up (red) and spin-down (blue) Q functions are superimposed. The average fidelities of the populations compared to theoretical predictions are 0.97 and 0.96 for $\hat{U}_0$ and $\hat{U}_1$, respectively. (c) Cavity Q functions after each step of the refocusing quantum walk with Bloch oscillations. The state refocuses after ten steps, as shown in the final frame for both $\hat{U}_0$ and $\hat{U}_1$. Refocusing fidelities (to the initial state) for $\hat{U}_0$ and $\hat{U}_1$ are 0.83 and 0.87, respectively.

In addition to the dynamical phase, upon traversing the Brillouin zone, the particle's spin winds around the Bloch sphere, encoding its path in the accumulated Berry phase [30],

$$\phi_B = i \int_{\mathrm{BZ}} \langle k, \vec{n}(k) | \partial_k | k, \vec{n}(k) \rangle dk = \pi \times \mathcal{W}, \qquad (2)$$

which thus becomes an observable manifestation of the winding number $\mathcal{W}$—the Hamiltonian's topological invariant. As one cannot directly observe the quantum mechanical phase of a wave function, measuring this Berry phase requires an interferometric approach. To this end, we perform the time-dependent walk with the cavity-qubit system initialized in a Schrödinger cat superposition of two coherent-state components: One component undergoes the walk, while the other is unaffected by the unitaries. The Berry phase thus appears as the relative phase between the two components and is observable via direct Wigner tomography.

The additional steps used in performing the time-dependent walks are shown in dashed boxes in Fig. 2(a). Beginning with either $\hat{U}_0$ or $\hat{U}_1$, we insert rotations by Δk about $\hat{\sigma}_z$ after each coin toss rotation $\hat{R}(\theta_1)$ and $\hat{R}(\theta_2)$. In contrast to the original operations comprising $\hat{U}_0$ and $\hat{U}_1$, the rotation angle Δk varies in time. Since a $\hat{\sigma}_z$ rotation is equivalent to a translation of the underlying Hamiltonian in quasimomentum space [24], this time-varying rotation angle implements a digital Bloch oscillation. We choose Δk to vary in steps of $\pi/10$ from 0 to π, traversing the Brillouin zone exactly once.

Populations resulting from the time-dependent walks (with the system initialized in a single coherent state) are shown in Fig. 2(c). Unlike the ballistic dynamics resulting from the original walks, the Bloch oscillation (traversal of the Brillouin zone) causes the walker wave function to refocus [25–28] to both its initial position and spin state. The intuition underlying this refocusing is that both the dynamical and Berry phases accumulated by each quasimomentum component of the walker is identical upon full

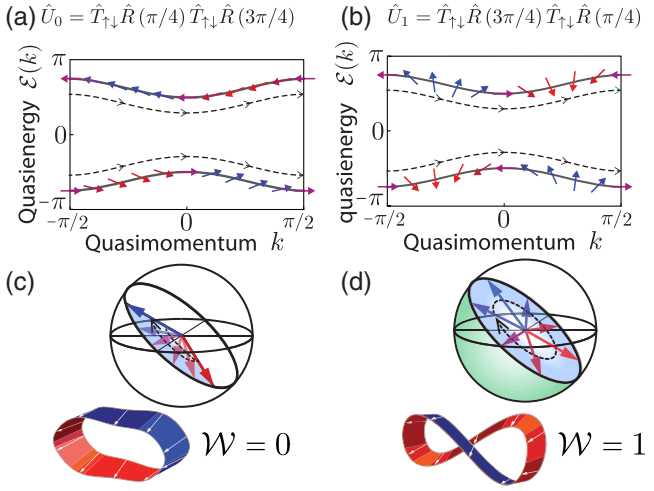

FIG. 3. Topological classes of split-step quantum walks. Calculated band structures, quasienergy ϵ versus quasimomentum k, corresponding to the two walks we perform in the experiment, $\hat{U}_0 = \hat{T}_{\uparrow\downarrow}\hat{R}(\pi/4)\hat{T}_{\uparrow\downarrow}\hat{R}(3\pi/4)$ (a) and $\hat{U}_1 = \hat{T}_{\uparrow\downarrow}\hat{R}(3\pi/4)\hat{T}_{\uparrow\downarrow}\hat{R}(\pi/4)$ (b). Though the energy bands of the two walks are identical, they are topologically distinct, with the topology given by the winding of $\vec{n}(k)$ as k varies through the Brillouin zone, shown in diagrams (c) and (d). In diagram (c), the trivial case $\hat{U}_0$, $\vec{n}(k)$ does not complete a full revolution around the Bloch sphere, while in the topological case $\hat{U}_1$ diagram (d), it does perform a full revolution. This also provides a direct connection to the Berry phase, as for a spin-1/2 system the Berry phase is simply half the subtended solid angle of the Bloch sphere path. A schematic representation of the variation of $\vec{n}(k)$ is shown by the ribbons below the Bloch spheres. The arrows on these strips point in the direction of $\vec{n}(k)$. Analogous to the number of twists in closed ribbons, winding numbers are quantized and robust to local perturbations.

traversal [19,24]. In practice, we observe refocusing fidelities greater than 80%, limited by incomplete adiabaticity and experimental imperfections.

Having verified the refocusing behavior of the time-dependent quantum walks, we initialize the cavity-qubit system in a Schrödinger cat state to measure the accumulated Berry phase [19]. One component of the cat is precisely the initial state of the previous walks, $|\beta,\uparrow\rangle$. The other component is $|0,f\rangle$, where the cavity is in its ground (vacuum) state and the transmon is in its second excited state [14], $|f\rangle$. Shelving the vacuum component of the cat in the $|f\rangle$ state renders it immune to the coin-toss rotations, as the $|f\rangle \leftrightarrow |\downarrow\rangle$ transition is far detuned (225 MHz) from the $|\uparrow\rangle \leftrightarrow |\downarrow\rangle$ transition. Thus, this component of the cat lies dormant during the walk, acting as a phase reference for the observation of the Berry phase. Our method of preparing the cat, a modification of the protocol introduced in Ref. [31], is shown in Fig. 4(a). With the cat initialized, we perform the time-dependent walk over a full Bloch oscillation, applying the same set of pulses that resulted in the final frames of Fig. 2(c). After the

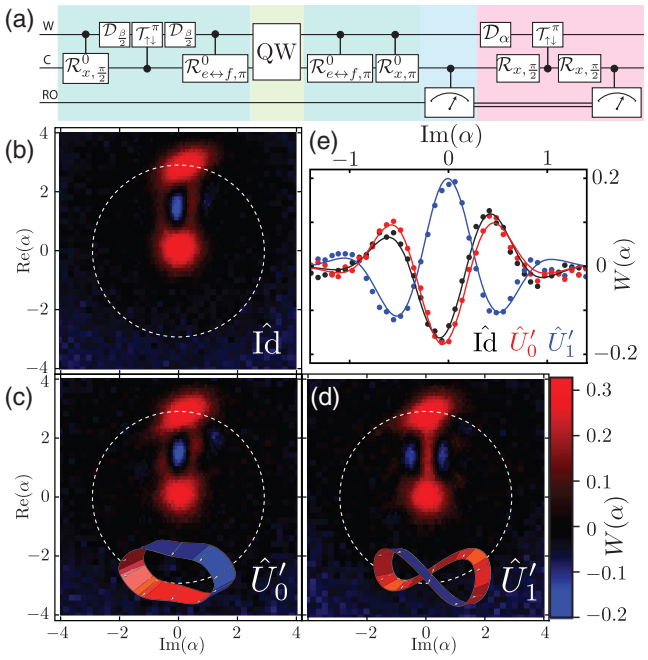

FIG. 4. Winding number measurement via direct Wigner tomography of refocused Schrödinger cat states. (a) Protocol for measuring topology via a time-dependent walk (Bloch oscillations). The Schrödinger cat state is first prepared (blue), after which the ten-step refocusing quantum walk is performed (green). The qubit and cavity state are then disentangled, the qubit state is purified (blue), and direct Wigner tomography on the cavity state is performed (pink). Wigner tomography of (b) the cat undergoing no quantum walk, (c) the cat after undergoing the trivial $\hat{U}_0$ walk, and (d) the cat after undergoing the topological $\hat{U}_1$ walk. Fidelities of these resulting cat states compared to pure cat states are 0.68, 0.69, and 0.67, respectively. (e) A cut of the Wigner function, showing the fringes that encode the relative phase between the two cat components for no walk (black), a trivial walk (red), and a topological walk (blue). The relative phase corresponds to the phase of the measured interference fringes following the relation $A\exp[-2|\mathrm{Im}(\alpha)|^2]\cos[2\sqrt{\bar{n}}\mathrm{Im}(\alpha)+\phi]$, where A, ϕ are the amplitude and phase of the fringes. The Berry phase—captured by the phase difference between the topological and the trivial walks—is $\phi_B = 1.05\pi \pm 0.06\pi$ in experiment, consistent with the theoretical expectations of π.

walking component of the cat refocuses, we disentangle the qubit from the cavity with the operation $|0,f\rangle \rightarrow |0,\uparrow\rangle$. This leaves the oscillator in the state

$$|\psi\rangle = |0\rangle - e^{i\phi_B}|\beta\rangle, \tag{3}$$

where ϕ_B is the Berry phase.

While Q tomography lends itself well to measuring coherent-state occupations, coherences between these states are largely invisible in this representation. To measure the Berry phase, we therefore apply direct Wigner tomography to the final cavity state [19,31,32]. As Figs. 4(b)–4(d) show, the Wigner functions of two-component cat states display interference fringes, whose phase directly encodes the

relative phase between the dormant ($|0, f\rangle$) and walking ($|\beta, \uparrow\rangle$) components of the cat. Figures 4(c) and 4(d) display the measured Wigner functions for both split-step walks. In the topologically trivial phase [Fig. 4(c)], the interference fringes do not acquire any phase shift after the walk, besides a small offset due to technical imperfections. For the topologically nontrivial walk [Fig. 4(d)], however, the fringes visibly shift [Fig. 4(e)], corresponding to an acquired phase of $\phi_B = 1.05\pi \pm 0.06\pi$. The topologies of the Hamiltonians that generate the walks are thereby clearly imprinted on the Wigner functions of the refocused states. A key feature of such topology is its robustness to all perturbations that do not close the spectral gap. To this end, we have performed an additional pair of quantum walks, $\hat{U}'_0 = \hat{U}_W(0.64\pi, 0.28\pi)$ and $\hat{U}'_1 = \hat{U}_W(0.28\pi, 0.64\pi)$, which are continuously deformable from the original walks. In this case, line cuts of the two Wigner functions yield an extracted Berry phase difference of $\Delta\phi = 1.07\pi \pm 0.09\pi$ [19]. Thus, we have successfully observed, in a systematic fashion, both phases in the canonical BDI topological insulator class [4,5].

In conclusion, we have demonstrated a novel quantum-walk-based simulator capable of emulating topological phases and directly measuring their associated topological invariants. These invariants underlie phenomena such as topologically protected edge states [18], which have been previously observed with quantum walks. In directly measuring the associated topological invariants, our work provides the missing piece of this bulk-edge correspondence for quantum walks.

In addition to the measurement of the topological invariant, this work also represents the first realization of a quantum walk in the phase space of a microwave cavity. This effective simulation of dynamics on a lattice—using only a single cavity and single qubit—demonstrates that the large, controllable Hilbert space associated with the cavity QED system is able to perform quantum simulation of systems that have traditionally been the purview of cold atomic systems. Besides simulation, the quantum walk on a circle, which we have realized here, is also of interest from the point of view of algorithms [33], with potential applications in sampling.

Looking towards future work, a direct extension of our protocol would be to realize multidimensional quantum walks [17], which have the potential to simulate novel topological insulators in two and three dimensions (e.g., the Hopf insulator) [34]. Since our quantum walk happens in the phase space of a cavity, the effective dimensionality can be increased simply by coupling the walker qubit to extra microwave resonators. The advantage of using such a "synthetic" lattice is that its dimensionality is not limited by that of the embedding space.

In higher dimensions, various versions of discrete-time quantum walks have been studied. For instance, it is possible to realize all known topological classes in two dimensions using walks with a single two-state walker [17]. A single step of these walks consists of multiple spin-dependent translation steps in different directions, necessitating the modification in time of the dispersive shifts. Using the current Bloch-oscillating protocol, the 2D Brillouin zone can be swept out in stripes, whereby a measurement of the Berry phase acquired along each stripe allows the extraction of the Chern number [35].

The generalization of quantum-walk-based protocols to measurements of many-body topological invariants represents an exciting frontier at the interface of topology, interactions, and quantum simulation [36,37].

The authors acknowledge discussions with David Toyli, Chris Macklin, Kevin Fischer, Mark Rudner, Eugene Demler, and Carlos Navarette-Benloch for motivating the use of a refocusing quantum walk. V. V. R. and L. S. M. acknowledge funding via the National Science Foundation. N. Y. Y. acknowledges support from the Miller Institute for Basic Research in Science. This research is supported in part by the U.S. Army Research Office (ARO) under Grant No. W911NF-15-1-0496 and by the AFOSR under Grant No. FA9550-12-1-0378.

[1] E. M. Lifshitz and L. P. Pitaevskii, *Statistical Physics: Theory of the Condensed State* (Elsevier, Vancouver, 2013), Vol. 9.
[2] J. E. Moore, *The Birth of Topological Insulators*, Nature (London) **464**, 194 (2010).
[3] M. Z. Hasan and C. L. Kane, *Colloquium: Topological Insulators*, Rev. Mod. Phys. **82**, 3045 (2010).
[4] A. Kitaev, *Periodic Table for Topological Insulators and Superconductors*, AIP. Conf. Ser. **1134**, 22 (2009).
[5] A. P. Schnyder, S. Ryu, A. Furusaki, and A. W. Ludwig, *Classification of Topological Insulators and Superconductors in Three Spatial Dimensions*, Phys. Rev. B **78**, 195125 (2008).
[6] Y. Aharonov, L. Davidovich, and N. Zagury, *Quantum Random Walks*, Phys. Rev. A **48**, 1687 (1993).
[7] J. Kempe, *Quantum Random Walks: An Introductory Overview*, Contemp. Phys. **44**, 307 (2003).
[8] P. M. Preiss, R. Ma, M. E. Tai, A. Lukin, M. Rispoli, P. Zupancic, Y. Lahini, R. Islam, and M. Greiner, *Strongly Correlated Quantum Walks in Optical Lattices*, Science **347**, 1229 (2015).
[9] E. Farhi and S. Gutmann, *Quantum Computation and Decision Trees*, Phys. Rev. A **58**, 915 (1998).
[10] A. Ambainis, *Quantum Walk Algorithm for Element Distinctness*, SIAM J. Comput. **37**, 210 (2007).
[11] A. M. Childs, *Universal Computation by Quantum Walk*, Phys. Rev. Lett. **102**, 180501 (2009).
[12] H. Paik, D. I. Schuster, L. S. Bishop, G. Kirchmair, G. Catelani, A. P. Sears, B. R. Johnson, M. J. Reagor, L. Frunzio, L. I. Glazman *et al.*, *Observation of High Coherence in Josephson Junction Qubits Measured in a Three-Dimensional Circuit QED Architecture*, Phys. Rev. Lett. **107**, 240501 (2011).

[13] B. C. Sanders, S. D. Bartlett, B. Tregenna, and P. L. Knight, *Quantum Quincunx in Cavity Quantum Electrodynamics*, Phys. Rev. A **67**, 042305 (2003).
[14] J. Koch, T. M. Yu, J. Gambetta, A. A. Houck, D. I. Schuster, J. Majer, A. Blais, M. H. Devoret, S. M. Girvin, and R. J. Schoelkopf, *Charge-Insensitive Qubit Design Derived from the Cooper Pair Box*, Phys. Rev. A **76**, 042319 (2007).
[15] P. Xue, B. C. Sanders, A. Blais, and K. Lalumière, *Quantum Walks on Circles in Phase Space via Superconducting Circuit Quantum Electrodynamics*, Phys. Rev. A **78**, 042334 (2008).
[16] B. C. Travaglione and G. J. Milburn, *Implementing the Quantum Random Walk*, Phys. Rev. A **65**, 032310 (2002).
[17] T. Kitagawa, M. S. Rudner, E. Berg, and E. Demler, *Exploring Topological Phases with Quantum Walks*, Phys. Rev. A **82**, 033429 (2010).
[18] T. Kitagawa, M. A. Broome, A. Fedrizzi, M. S. Rudner, E. Berg, I. Kassal, A. Aspuru-Guzik, E. Demler, and A. G. White, *Observation of Topologically Protected Bound States in Photonic Quantum Walks*, Nat. Commun. **3**, 882 (2012).
[19] See Supplemental Material at http://link.aps.org/supplemental/10.1103/PhysRevX.7.031023 for additional details on cavity field representations, the experimental implementation of Bloch oscillations and topological features of quantum walks.
[20] J. K. Asbóth and H. Obuse, *Bulk-Boundary Correspondence for Chiral Symmetric Quantum Walks*, Phys. Rev. B **88**, 121406 (2013).
[21] M. Atala, M. Aidelsburger, J. T. Barreiro, D. Abanin, T. Kitagawa, E. Demler, and I. Bloch, *Direct Measurement of the Zak Phase in Topological Bloch Bands*, Nat. Phys. **9**, 795 (2013).
[22] M. Aidelsburger, M. Lohse, C. Schweizer, M. Atala, J. T. Barreiro, S. Nascimbene, N. Cooper, I. Bloch, and N. Goldman, *Measuring the Chern Number of Hofstadter Bands with Ultracold Bosonic Atoms*, Nat. Phys. **11**, 162 (2015).
[23] P. Roushan, C. Neill, Y. Chen, M. Kolodrubetz, C. Quintana, N. Leung, M. Fang, R. Barends, B. Campbell, Z. Chen *et al.*, *Observation of Topological Transitions in Interacting Quantum Circuits*, Nature (London) **515**, 241 (2014).
[24] V. V. Ramasesh, E. Flurin, M. S. Rudner, I. Siddiqi, and N. Y. Yao, *Direct Probe of Topological Invariants Using Bloch Oscillating Quantum Walks*, Phys. Rev. Lett. **118**, 130501 (2017).
[25] M. C. Bañuls, C. Navarrete, A. Pérez, E. Roldán, and J. C. Soriano, *Quantum Walk with a Time-Dependent Coin*, Phys. Rev. A **73**, 062304 (2006).
[26] M. Genske, W. Alt, A. Steffen, A. H. Werner, R. F. Werner, D. Meschede, and A. Alberti, *Electric Quantum Walks with Individual Atoms*, Phys. Rev. Lett. **110**, 190601 (2013).
[27] R. Matjeschk, A. Ahlbrecht, M. Enderlein, C. Cedzich, A. Werner, M. Keyl, T. Schaetz, and R. Werner, *Quantum Walks with Nonorthogonal Position States*, Phys. Rev. Lett. **109**, 240503 (2012).
[28] C. Cedzich, T. Rybár, A. H. Werner, A. Alberti, M. Genske, and R. F. Werner, *Propagation of Quantum Walks in Electric Fields*, Phys. Rev. Lett. **111**, 160601 (2013).
[29] F. Bloch, *Über die Quantenmechanik der Elektronen in Kristallgittern*, Z. Phys. **52**, 555 (1929).
[30] J. Zak, *Berrys Phase for Energy Bands in Solids*, Phys. Rev. Lett. **62**, 2747 (1989).
[31] B. Vlastakis, G. Kirchmair, Z. Leghtas, S. E. Nigg, L. Frunzio, S. M. Girvin, M. Mirrahimi, M. H. Devoret, and R. J. Schoelkopf, *Deterministically Encoding Quantum Information Using 100-Photon Schrödinger Cat States*, Science **342**, 607 (2013).
[32] J. Raimond and S. Haroche, *Exploring the Quantum* (Oxford University Press, New York, 2006), Vol. 82, p. 86.
[33] S. E. Venegas-Andraca, *Quantum Walks: A Comprehensive Review*, Quantum Inf. Process. **11**, 1015 (2012).
[34] J. E. Moore, Y. Ran, and X.-G. Wen, *Topological Surface States in Three-Dimensional Magnetic Insulators*, Phys. Rev. Lett. **101**, 186805 (2008).
[35] D. A. Abanin, T. Kitagawa, I. Bloch, and E. Demler, *Interferometric Approach to Measuring Band Topology in 2D Optical Lattices*, Phys. Rev. Lett. **110**, 165304 (2013).
[36] A. Schreiber, A. Gabris, P. P. Rohde, K. Laiho, M. Stefanak, V. Potocek, C. Hamilton, I. Jex, and C. Silberhorn, *A 2D Quantum Walk Simulation of Two-Particle Dynamics*, Science **336**, 55 (2012).
[37] F. Grusdt, N. Y. Yao, D. Abanin, M. Fleischhauer, and E. Demler, *Interferometric Measurements of Many-Body Topological Invariants Using Mobile Impurities*, Nat. Commun. **7**, 11994 (2016).